High-Speed Parameter Estimation Algorithms For Nonlinear Smart Materials

Jon M. Ernstberger*and Ralph C. Smith†

Center for Research in Scientific Computation
Department of Mathematics
North Carolina State University
Raleigh, NC 27695

ABSTRACT

A fundamental step in the model construction for ferroelectric, ferromagnetic, and ferroelastic materials is the estimation or identification of material parameters given measurements of the material response. Moreover, actuator and/or material properties may be a function of operating conditions which can necessitate the re-estimation of parameters if conditions change significantly. In this paper, we focus on the development of highly robust and efficient identification algorithms for use in industrial, aeronautic and aerospace applications. Following a discussion of present and future applications, we summarize the homogenized energy model used to characterize hysteresis and constitutive nonlinearities in these compounds. We next discuss the parameter estimation problem and detail algorithms used to speed implementation. The validity of the framework is illustrated through comparison with experimental data.

1. INTRODUCTION

Smart materials exhibit unique actuator and sensor capabilities for a range of aerospace, aeronautic, industrial and DoD applications. Applications of smart materials include transducers, vibration attenuation or damping, and energy harvesting based upon vibration or physical stresses applied to the materials. For both actuating and sensing, transducers employing smart material compounds are often more efficient than their classical counterparts.

Ferromagnetic materials exhibit actuator behavior in response to an applied magnetic field and sensor capabilities in response to mechanical deformations. However, due to nonuniform moment switching, these materials behave nonlinearly in response to input fields or deformations. We summarize one application of the ferromagnetic material Terfenol-D. As depicted in Figure 1, a Terfenol-D rod is used as the active material to drive a cutting head for high speed milling. In response to an applied magnetic field, the Terfenol-D rod length changes which in turn alters the position of the cutting head. The nonlinear material behavior creates difficulty when attempting to mill objects to a specified shape within small tolerances. This necessitates the development of control laws that take into account the hysteretic material behavior.

The need for such a controller necessitates an accurate model representation. Unfortunately, environmental change can alter the properties of the Terfenol-D rod and actuator behavior. These varying material properties can mandate frequent parameter re-estimations after deploying these devices to industry. These estimations must be performed in a manner which do not greatly hinder production rates while yielding parameter values which are physical and result in accurate device quantification.

Using the milling device of Figure 1 as motivation for this research, we summarize the model formulation which characterizes Terfenol-D magnetization and rod tip displacement in Section 2. We then describe the

*jmernstb@ncsu.edu
†rsmith@eos.ncsu.edu

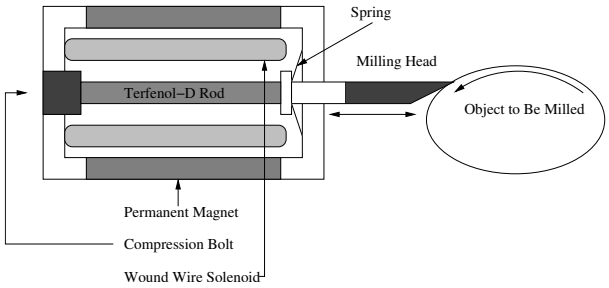

Figure 1. The use of a Terfenol-D rod as an actuator in a typical industrial milling application.

parameter estimation problem in Section 3 and the processes employed to estimate these parameters on-site with low runtimes in Section 4. Finally, in Section 5, we discuss the use of varying optimization routines and their implementations in order to perform quick and robust parameter estimations.

2. MODEL FRAMEWORK

We employ the homogenized energy model detailed in [7] in the framework of magnetization with magnetic field inputs. We employ energy relations at the lattice level to determine average material magnetization using statistical mechanics principles. Material inhomogeneities are then incorporated by assuming that certain material properties are manifestations of underlying distributions. Finally we assume that the transducer can be modeled as a one-dimensional rod. With assumptions on internal stress-strain relationships and by balancing rod tip forces we write rod tip displacement as a solvable first-order system of ordinary differential equations.

2.1. Homogenized Energy Model

As detailed in [7], we employ the piecewise quadratic Helmholtz relation

$$\psi(M) = \begin{cases} \frac{1}{2}\eta\left(M + M_R\right)^2 & M \leq -M_I \\ \frac{1}{2}\eta\left(M - M_R\right)^2 & M \geq M_I \\ \frac{1}{2}\eta\left(M_I - M_R\right)\left(\frac{M^2}{M_I} - M_R\right) & |M| \leq M_I \end{cases} \tag{1}$$

to quantify the internal energy due to moment reorientation. Here M_R is the remanent magnetization, η is the reciprocal of the slope of the $H - M$ relation, and M_I is the positive inflection point of (1). The Gibbs energy

$$G(H, M) = \psi(M) - HM \tag{2}$$

incorporates elastic and electrostatic work. The Boltzmann relation

$$\mu(G) = Ce^{-GV/kT} \tag{3}$$

is used to balance the Gibbs energy G and the relative thermal energy kT/V where k is Boltzmann's constant, V is volume and C is chosen to ensure integration to one.

The likelihoods of moments switching from positive to negative and negative to positive orientation are

$$p_{+-} = \frac{1}{\mathcal{T}(t)} \frac{\int_{M_I-\epsilon}^{M_I} e^{-G(H,M)V/kT} dM}{\int_{M_I-\epsilon}^{\infty} e^{-G(H,M)V/kT} dM} \quad , \quad p_{-+} = \frac{1}{\mathcal{T}(t)} \frac{\int_{-M_I}^{-M_I+\epsilon} e^{-G(H,M)V/kT} dM}{\int_{-\infty}^{-M_I+\epsilon} e^{-G(H,M)V/kT} dM} \tag{4}$$

where ϵ is a small positive constant and $\mathcal{T}$ is the reciprocal of the frequency at which moments attempt to switch. Let x_+ and x_- denote the fraction of total moments respectively having positive and negative

orientations. These ratios are governed by the pair of differential equations

$$\dot{x}_+ = -p_{+-}x_+ + p_{-+}x_- \qquad \dot{x}_- = -p_{-+}x_- + p_{+-}x_+ \tag{5}$$

where $x_+ + x_- = 1$. Given (3), the expected magnetizations $\langle M_+ \rangle$ and $\langle M_- \rangle$ are

$$\langle M_+ \rangle = \frac{\int_{M_I}^{\infty} M e^{G(H,M)V/kT} dM}{\int_{M_I}^{\infty} e^{G(H,M)V/kT} dM} \quad , \quad \langle M_- \rangle = \frac{\int_{-\infty}^{-M_I} M e^{G(H,M)V/kT} dM}{\int_{-\infty}^{-M_I} e^{G(H,M)V/kT} dM}. \tag{6}$$

For a uniform input field H, the local average magnetization is given by

$$\bar{M} = x_+ \langle M_+ \rangle + x_- \langle M_- \rangle. \tag{7}$$

The macroscopic magnetization of a structure can be denoted as

$$[M(H)](t) = \int_0^{\infty} \int_{-\infty}^{\infty} \nu_1(H_c)\nu_2(H_I) \left[\bar{M}(H + H_I; H_c, \xi)\right](t) dH_I dH_c \tag{8}$$

when we assume that material inhomogeneities and variable effective fields can be described as underlying distributions. We denote the densities associated with these distributions as $\nu_1(H_c)$ and $\nu_2(H_I)$ and make the following assumptions:

$$\begin{aligned} &1.)\ \nu_1(x) \text{ is only defined for } x > 0; \\ &2.)\ \nu_2(-x) = \nu_2(x) \text{ for density symmetry;} \\ &3.)\ |\nu_1(x)| \le c_1 e^{-a_1 x} \text{ and } |\nu_2(x)| \le c_2 e^{-a_2|x|}. \end{aligned} \tag{9}$$

The third requirement in (9) guarantees density non-negativity and exponential decay as distance from the density mean increases while c_1, c_2, a_1 and a_2 remain positive.

Equation (8) can be discretized using a composite quadrature rule as

$$[M(H)](t) \approx \sum_{i=1}^{N_i} \sum_{j=1}^{N_j} \nu_1(H_{c_i})\nu_2(H_{I_j}) \left[\bar{M}(H_{I_j} + H; H_{c_i}, \xi_j)\right](t) v_i w_j \tag{10}$$

where H_{c_i} and H_{I_j} are the quadrature nodes, v_i and w_j are the quadrature weights associated with the quadrature points, and N_i, N_j are the number of quadrature points; see [7] for details.

2.2. Lumped Rod Model

We characterize the behavior of the Terfenol-D rod as connected to the cutting mechanism of the milling device shown in Figure 1 by the simplified model depicted in Figure 2. This allows for a simple one-dimensional lumped rod model formulation.

As detailed in [7], we employ the constitutive relation

$$\sigma = Y\varepsilon + C\dot{\varepsilon} - a_1(M(H) - M_0) - a_2(M(H) - M_0)^2 \tag{11}$$

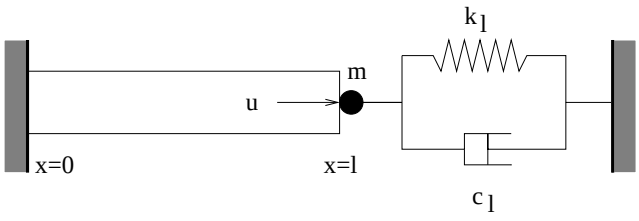

Figure 2. Representation of the Terfenol-D rod in a typical actuator design.

where M is given by (8), Y is the Young's modulus, a_1 and a_2 are coupling coefficients, and C is the Kelvin-Voigt damping coefficient. We assume that strain is uniform along the length of the rod so that strains have the form

$$\varepsilon(t) = \frac{u_\ell(t)}{\ell} \tag{12}$$

where $u_\ell(t)$ is rod tip position at time t and ℓ is the rod length. Balancing the forces of the rod σA (where A is cross-sectional area and ρ is density) with those of the restoring mechanism yields

$$\rho A\ell\ddot{u}_\ell(t) + \frac{CA}{\ell}\dot{u}_\ell(t) + \frac{YA}{\ell}u_\ell(t) = -m_\ell\ddot{u}_\ell(t) - c_\ell\dot{u}_\ell(t) - k_\ell u_\ell(t) + Aa_1\left[M(H) - M_0\right] + Aa_2\left[M(H) - M_0\right]^2. \tag{13}$$

This can be reformulated as the vector system

$$\frac{d}{dt}\begin{bmatrix} u_\ell \\ \dot{u}_\ell \end{bmatrix} = \begin{bmatrix} 0 & 1 \\ -\frac{k}{m} & -\frac{c}{m} \end{bmatrix}\begin{bmatrix} u_\ell \\ \dot{u}_\ell \end{bmatrix} + \begin{bmatrix} 0 \\ \frac{1}{m} \end{bmatrix}\tilde{a}_1\left[M(H)(t) - M_0\right] + \tilde{a}_2\left[M(H)(t) - M_0\right]^2 \tag{14}$$

where

$$m = \rho A\ell + m_\ell, \quad c = \frac{CA}{\ell} + c_\ell, \quad k = \frac{YA}{\ell} + k_\ell, \quad \tilde{a}_1 = Aa_1, \quad \tilde{a}_2 = Aa_2. \tag{15}$$

Note that m_ℓ, c_ℓ, and k_ℓ are material properties from the attachment to the rod end as shown in Figure 2. Details regarding the derivation of this model is given in [7, 8]. In the case of the Terfenol-D actuator of Figure 1, the input to the lumped rod model is magnetization and the point about which the material is magnetized is denoted by M_0 which varies for each application.

3. PARAMETER ESTIMATION

We use the model as given by (8) and (14) which characterizes rod tip displacement u_ℓ to estimate the displacement of a smart-material driven actuator with actuator displacement data $\hat{u}_\ell$. The parameter estimation problem can be formulated as a least-squares objective functional of the form

$$\min_{\mathbf{q}} J(\mathbf{q}) = \min_{\mathbf{q}} \frac{1}{2}\sum_{i=1}^{N}\left|u_\ell(\mathbf{q}, H_i) - \hat{u}_\ell(H_i)\right|^2 \tag{16}$$

where

$$\mathbf{q} = \left[\tfrac{c}{m}, \tfrac{k}{m}, \tilde{a}_1, \tilde{a}_2, P_R, \eta, \tau(T), \gamma, \mathbf{q}_{density}\right]^T. \tag{17}$$

Here $\gamma = \frac{V}{kT}$ where V is material volume, k is Boltmann's constant, and T is the temperature. The parameters $\mathbf{q}_{density}$ describe the densities used in the least-square fit to data. Note that $\mathbf{q} \in \mathbb{R}^+_{m\times 1}$ (making this a bounded optimization problem) where m is the dimension of $\mathbf{q}$ which varies upon density and quadrature rule choices.

One choice for the coercive and interaction field densities are the lognormal and normal relations

$$\nu_1(H_c) = c_1 e^{-\left[\ln\left(H_c/\bar{H}_c\right)/2c\right]^2} \tag{18}$$

$$\nu_2(H_i) = c_2 e^{-H_I^2/2b^2}. \tag{19}$$

In this case, the parameters to be estimated are given as

$$\mathbf{q} = \left[\tfrac{c}{m}, \tfrac{k}{m}, \tilde{a}_1, \tilde{a}_2, P_R, \eta, \tau(T), \gamma, b, \bar{H}_c, c\right]^T. \tag{20}$$

If we use a general density approximation in which we estimate all of the quadrature values in (10), then

$$\mathbf{q} = \left[\tfrac{c}{m}, \tfrac{k}{m}, \tilde{a}_1, \tilde{a}_2, P_R, \eta, \tau(T), \gamma, \{\nu_2\left(H_{I_j}\right)\}, \{\nu_1(H_{c_i})\}\right]^T \tag{21}$$

where $\{\nu_2\left(H_{I_j}\right)\}$ is the set of interaction field density values defined for $H_{I_j} \geq 0$. The set $\{\nu_1(H_{c_i})\}$ is the coercive field density values. Results of parameter estimations using normal/lognormal and generally distributed interaction and coercive field densities are given in Figure 3.

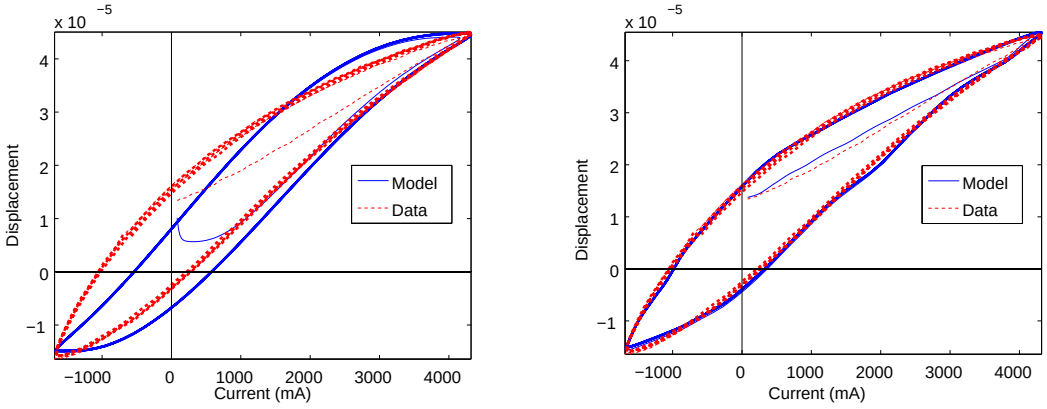

Figure 3. (a) Fit to data with 100 Hz current input using normally distributed interaction and lognormally distributed coercive field densities. (b) Fit to data with 100 Hz current input using generally distributed interaction and coercive field densities.

4. IMPLEMENTATION ENHANCEMENTS

4.1. Galerkin Expansion Approximation to General Densities

Performing parameter estimation with lognormal coercive and normal interaction field densities is fast ($\mathbf{q}$ has eleven components for this example) and the fits to data are smooth although often only moderately accurate as shown in Figure 3(a). Parameter estimates using general coercive and interaction field densities perform well (lower least-squares residual), as shown in Figure 3(b), but may take significantly longer. For example, in the case of four-point Gaussian quadrature, the dimension of $\mathbf{q}$ is $8+6N$ for N quadrature intervals. For large N, the dimension of the parameter space is quite large resulting in long estimation runtimes. Finally, the general densities are often not smooth and may be multi-modal or even non-decaying which are both non-physical attributes.

By using a Galerkin expansion to approximate the interaction and coercive field densities, we can reduce estimation runtime by reducing the dimension of the parameter space. We also approximate our densities with polynomials which results in an increased smoothness to the fit of the data. Galerkin expansions of the densities have the form

$$\nu_1(H_c) = \sum_{i=0}^{n} \alpha_i \phi_i(H_c) \quad \text{and} \quad \nu_2(H_I) = \sum_{j=0}^{m} \beta_j \phi_j(H_I) \tag{22}$$

where the α_i and β_j are coefficients and ϕ_i, ϕ_j are basis functions. One choice is a linear basis function which is piecewise continuous and defined as

$$\phi_i(x) = \begin{cases} \frac{x-x_{i-1}}{h}, & x \in [x_{i-1}, x_i) \\ \frac{x_{i+1}-x}{h}, & x \in [x_i, x_{i+1}) \\ 0, & \text{else.} \end{cases} . \tag{23}$$

Another basis choice is the cubic B-spline which is defined piecewise continuously as

$$\phi_i(x) = \frac{1}{h^3} \begin{cases} (x-x_{i-2})^3, & x \in [x_{i-2}, x_{i-1}) \\ h^3 + 3h^2(x-x_{i-1}) + 3h(x-x_{i-1})^2 - 3(x-x_{i-1})^3, & x\,[x_{i-1}, x_i) \\ h^3 + 3h^2(x_{i+1}-x) + 3h(x_{i+1}-x)^2 - 3(x_{i+1}-x)^3, & x\,[x_i, x_{i+1}) \\ (x_{i+2}-x)^3, & x \in [x_{i+1}, x_{i+2}) \\ 0, & \text{else} \end{cases} \tag{24}$$

as defined in [7]. The result of the use of the cubic spline is increased smoothness of the densities which translates directly to a smoother fit.

In both cases, the parameters to be estimated can be written as

$$\mathbf{q} = \left[\tfrac{c}{m}, \tfrac{k}{m}, \tilde{a}_1, \tilde{a}_2, P_R, \eta, \tau(T), \gamma, \{\beta_j\}, \{\alpha_i\}\right]^T \tag{25}$$

where $\{\beta_j\}$ is the set of coefficients corresponding to the non-negative domain of the interaction field density and $\{\alpha_i\}$ is the set of all coefficients of the Galerkin expansion to the coercive field density. This reduces the size of $\mathbf{q}$ to approximately $8 + 3N/2$ for N composite quadrature intervals regardless of the quadrature rule in use. With only positivity constraints (on the linear expansion), the densities may still be non-physical.

4.2. Density Constraints

In previous discussion, parameter constraints consisted solely of lower bounds on the model parameters and density parameters (normal/lognormal, general, or linear Galerkin expansion since the coefficients for the cubic expansion can be negative). We now enforce the constraints summarized in (9).

We first require exponential decay of both the interaction and coercive field densities. In the case of the general densities or the linear Galerkin expansions, linear inequality constraints are easily demonstrated to yield this decay in simple form. For the interaction field the linear inequality constraints can be written as

$$-\nu_2(H_{I_j}) + \nu_2(H_{I_{j+1}}) \leq 0 \quad \text{and} \quad -\beta_p + \beta_{p+1} \leq 0. \tag{26}$$

where the range p and j vary depending on quadrature interval number and rule. For the coercive field density, if we recover the maximum value of that density from an initial estimate, we can impose constraints on increase and decrease of the density about the maximum value.

If we require the density to decay, we need to restrict the density values or the expansions to be zero at the ends of our interval of integration of (8). In the general densities or Galerkin expansion (linear or cubic) approximation to the densities, the last value is actually an entry in $\mathbf{q}$. We could formally write linear equality constraints to force these values to zero. However, in a constrained optimization routine, this is computationally difficult and prohibits convergence. Simply setting these end density values to zero and eliminating them from the parameter set to be estimated reduces the size of $\mathbf{q}$ to either $5 + 3N/2$ for the Galerkin expansions or $5 + 6N$ for the general densities case with four-point Gaussian quadrature.

For unconstrained optimization routines, additional penalty terms can be added to the objective functional to penalize undesired behavior such as negative density values or a lack of proper decay in the densities. These soft constraints can allow unconstrained routines to perform well if properly weighted in the objective functional. However, better rates of convergence have been observed using constrained optimization routines.

5. OPTIMIZATION ROUTINES

All presented results are the result of two parameter estimations. The first is an estimation using the normal interaction and lognormal coercive field density approximations. Assuming that we perform enough iterations and function evaluations to achieve a strong local minima, we take this value as a new initial estimate for the parameters to be used in fitting the model to strain data using either a general densities or Galerkin expansion approximation to the densities.

At this point an optimization routine must be employed which is sufficiently robust to accommodate significant actuator change yet is quick enough to be run intermittently without drastic reduction in production rates. These two goals are often in direct opposition to each other. Several deterministic and stochastic search methods were employed to achieve sufficiently robust yet quick estimation. We give brief discussions and results from the routines which performed best.

5.1. Sequential Quadratic Programming

Sequential quadratic programming is designed to take a constrained minimization problem and return the function minimum. The problem is typically formatted as

$$\begin{aligned} &\min_{\mathbf{q}\in\mathcal{Q}} J(\mathbf{q}) \\ \text{subject to } &c_i(\mathbf{q}) = 0 \quad \text{for } i = 1\dots m \\ &c_i(\mathbf{q}) \leq 0 \quad \text{for } i = m+1\dots n \end{aligned} \tag{27}$$

where $\mathcal{Q}$ is the parameter space and the $c_i(\mathbf{q})$ are linear or nonlinear functions providing constraints. The constrained objective functional is written as the Lagrangian

$$\mathcal{L}(\mathbf{q},\lambda) = J\mathbf{q}) + \sum_{i\in I_1} \lambda_i c_i(\mathbf{q}) \tag{28}$$

where the λ_i are Lagrange multipliers and the Lagrangian is subject to certain constraints. The Lagrangian is rewritten in terms of a Taylor expansion replacing the gradient with a finite differences approximation and the Hessian with either a finite differences approximation or Hessian update (such as BFGS as in [4]). Complete with constraints, our expansion is in the form of a quadratic programming problem. The solution to the QP subproblem is the step in a Newton iteration for both the parameter which is being estimated and the Lagrange multipliers. The process of solving the QP subproblem to update a Newton step is iteratively performed until either a preset iteration maximum is reached or some convergence criteria are met.

To make these methods more robust and hopefully globally convergent, a merit function, as described in [1], is included in the implementation of these SQP routines. When the iteration fails to converge normally, the merit function will be evaluated to compute a new estimate. If this estimate yields a lower objective functional value than the current iterate, this estimate is accepted as the new iterate. The images in Figure 4 are generated using the estimates from an SQP routine.

The results of using a SQP-based routine are given in Figure 4.

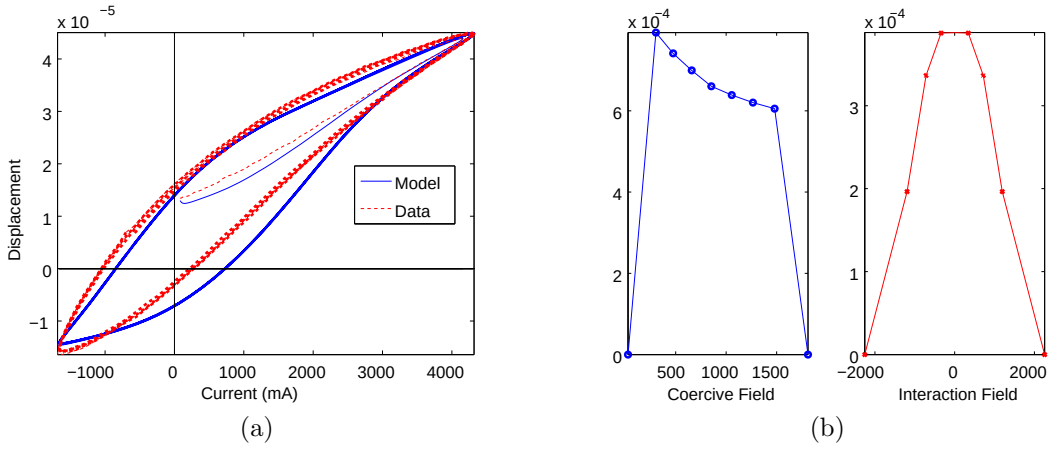

Figure 4. (a) Fit to data with 100 Hz current input using linear Galerkin expansion with eight quadrature intervals. (b) Densities as defined using the linear inequality constraints of Section 4.2.

5.2. Genetic Algorithms

Genetic algorithms are a class of optimization routines seeking to mimic nature's survival of the fittest. Most of these begin with some population of unequal initial estimates which are either uniformly distributed throughout the parameter space or created to initiate the algorithm at a certain point. Through some

predefined process, members of that population are chosen to be the analog of parents (with or without replacement) for a new *generation* in the population of estimates. Through the process of *crossover*, parameter values are swapped between these parents to form offspring. These offspring are also subjected to a process of *mutation* which takes into account natural random changes by either adding random normal noise or by converting the parameters to binary and performing bit swaps.

To achieve faster performance for the problem (27) with the GA, we create (*seed*) the initial population. By first performing the less accurate estimation (using normal interaction and lognormal coercive field densities) we have a new initial estimate to begin the population seeding. We add normally distributed noise to the new initial estimate with specific means and standard deviations. By seeding the initial population in such a way, we allow the GA to begin iterating with a population which is far better than the randomly produced population which covers the entire parameter space. Seeding the population also guarantees that the initial population meets our constraints. Finally as the GA gets very close to a minima, we export the best population member to the SQP routine mentioned above and allow the gradient-based search to continue the downhill search.

As shown in Figure 5, the GA/SQP combination is performed quickly (approximately 40 minutes) which is quite acceptable for less frequent parameter estimations. This estimation is better than just the result of the SQP due to obvious density smoothness and the stochasticity of the GA potentially allowing itself to work away from the minima of the seeded population to find a global minima. Assuming that the initial population is seeded correctly, the GA/SQP scheme appears to be the most robust algorithm of those considered.

More general details on the genetic algorithm can be found in [2], [3] and [9].

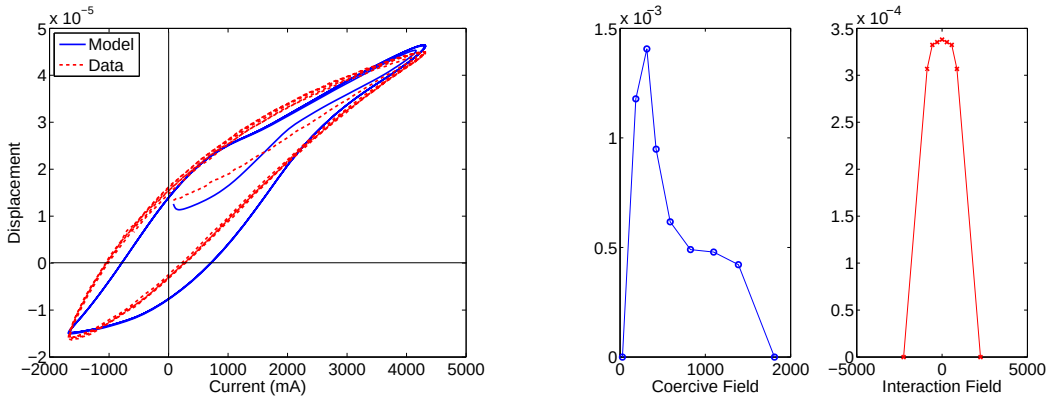

(a) (b)

Figure 5. (a) Data fit using the genetic algorithm with 100 Hz current input. Results are shown using four-point Gaussian quadrature with eight composite quadrature intervals. (b) Densities generated using the genetic algorithm, linear Galerkin expansions, and the constraints of Section 4.2.

5.3. Simulated Annealing

Simulated annealing is a global optimization routine founded in statistical mechanics. The Boltzmann distribution

$$\pi_T(\mathbf{q}) = \frac{e^{-\frac{E(\mathbf{q})}{kT}}}{\sum_{w \in Q} e^{-\frac{E(w)}{kT}}}, \tag{29}$$

as given in [2], yields the probability π_T that the system is in a configuration q given the energy $E(\mathbf{q})$ (standard objective functional) of the configuration. Here k is Boltzmann's constant, Q denotes the set of all possible configurations, and T is the system temperature. If we assume that at time t the system is in configuration $\mathbf{a}_1$ and generate another configuration $\mathbf{a}_2$ at time $t+1$ using the Metropolis stochastic

relaxation technique of [6] , then the ratio R is

$$R = \frac{\pi_T(\mathbf{a}_2)}{\pi_T(\mathbf{a}_1)} = e^{-\frac{E(\mathbf{a}_2)-E(\mathbf{a}_1)}{kT}}. \tag{30}$$

If $R > 1$, it is more likely that the system is in configuration $\mathbf{a}_2$ than $\mathbf{a}_1$, in which case $\mathbf{a}_2$ is accepted as the new configuration at time $t+1$. Otherwise, we then say that $\mathbf{a}_2$ is still accepted but with probability R. The temperature T at some time t is used to help tailor the performance of SA. This combination of temperature decrease (or increase) at necessary time intervals is known as an annealing schedule. Standard annealing schedules run the Metropolis algorithm at certain temperatures for set amounts of time as given in [5].

We enforce behavior in the form of soft constraints by appending penalties to our energy functional. Another difficulty to overcome is the randomness inherent to the SA process which does not allow for results to be repeated.

For this example, the simulated annealing algorithm required approximately 20 minutes to achieve the fit shown in Figure 6. This particular result had penalties in the energy functional placed upon density positivity, descent from the maximum of the interaction and coercive field densities, and a penalty on the smoothness of the densities beyond the standard least-squares penalty term.

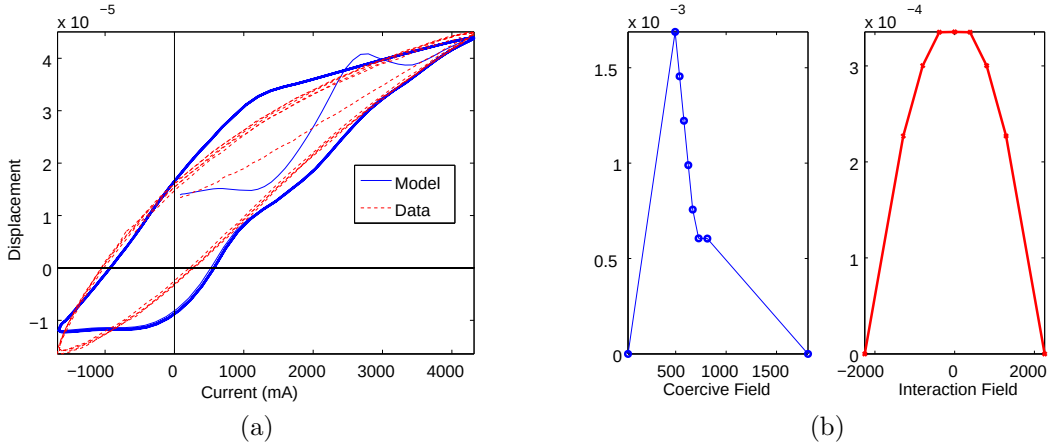

Figure 6. (a) Data with 100 Hz current input against a fit obtained using SA. (b) Linear density expansions with eight quadrature intervals and four point Gaussian quadrature. Constraints are enforced as in Section 4.2.

6. CONCLUDING REMARKS

We have characterized the magnetization of the Terfenol-D rod using the homogenized energy model and rod tip displacement using the lumped rod model of [7]. With current input and displacement data measured for the milling device, we solve the least squares fit-to-data problem using optimization techniques for parameter estimation.

To reduce computational times required for parameter estimation, Galerkin expansions were employed as approximations to interaction field and coercive field densities. Whereas more intensive than using normally distributed interaction field and lognormally distributed coercive field densities in the parameter estimates, the Galerkin expansions prove less computationally intensive than using general densities. The estimations using Galerkin expansions also yield smoother densities than those employing general densities which translate to a smoother fit to displacement data.

By using a fit-to-data where the interaction field density is normally distributed and the coercive field density is lognormally distributed, we achieve an accurate preliminary fit with a smaller parameter space,

which can be used to provide initial estimates for either general or Galerkin expansion densities. We then employ routines which attempt to achieve more accurate fits using merit functions or by stochastically allowing for a wide variety of change in parameter values while adhering to the predefined constraints. These constraints enforce decay and eliminate non-physical behavior thus yielding parameter values that are more physically accurate.

7. ACKNOWLEDGEMENTS

This research was supported in part by the Air Force Office of Scientific Research under the grant AFOSR-FA9550-04-1-0203.

REFERENCES

[1] P.T. Boggs and J.W. Tolle. Sequential quadratic programming for large-scale nonlinear optimization. *Journal of Computational and Applied Mathematics*, 124(1-2):123–137, 2000.

[2] L. Davis. *Genetic Algorithms and Simulated Annealing.* Morgan Kaufman Publishers, Inc.,95 First Street, Los Altos, CA 94022, 1987.

[3] J.H. Holland. Genetic algorithms and the optimal allocation of trials. *SIAM Journal of Computing*, 2(2), 1973.

[4] C.T. Kelley. *Iterative Methods for Optimization.* Society for Industrial and Applied Mathematics, 3600 University Science Center, Philadelphia, PA 19104-2688, 1999.

[5] S. Kirkpatrick, C.D. Gelatt Jr, and M.P. Vecchi. Optimization by Simulated Annealing. *Science*, 220(4598):671, 1983.

[6] N. Metropolis, A.W. Rosenbluth, M.N. Rosenbluth, and A.H Teller. Equation of State Calculations by Fast Computing Machines. *The Journal of Chemical Physics*, 21(6):1087–1092, 1953.

[7] R.C. Smith. *Smart Material Systems: Model Development.* Society for Industrial and Applied Mathematics, 2005.

[8] R.C. Smith, A.G. Hatch, T. De, M.V. Salapaka, R.C.H. del Rosario, and J.K. Raye. Model development for atomic force microscope stage mechanisms. *SIAM Journal on Applied Mathematics*, 66(6):1998–2026, 2006.

[9] J.C. Spall. *Introduction to Stochastic Search and Optimization: Estimation, Simulation and Control.* John Wiley and Sons, Inc., 2003.